

Estimation of seepage rates in a losing stream by means of fiber-optic high-resolution vertical temperature profiling

Tobias Vogt^{a,*}, Philipp Schneider^a, Lisa Hahn-Woernle^a, Olaf A. Cirpka^b

^aEawag – Swiss Federal Institute of Aquatic Science and Technology, Überlandstr. 133, 8600 Dübendorf, Switzerland

^bUniversity of Tübingen, Center for Applied Geoscience, Sigwartstr. 10, 72076 Tübingen, Germany

ARTICLE INFO

Article history:

Received 3 April 2009

Received in revised form 25 October 2009

Accepted 30 October 2009

This manuscript was handled by P. Baveye, Editor-in-Chief

Keywords:

River–groundwater interaction

Fiber-optic distributed temperature sensing

Time series analysis

Seepage flux

SUMMARY

Vertical temperature profiling in the river beds of losing streams has been shown to be useful in obtaining seepage rates. We present a method for high-resolution vertical temperature profiling in surface-water sediments for detailed quantification of seepage flux over depth and time. The method is based on fiber-optic distributed temperature sensing, in which temperature profiles along an optical fiber are obtained by making use of Raman scattering. An optical fiber was wrapped around a 2 in. PVC tube and installed vertically within the streambed sediment. The wrapping transfers the spatial resolution along the fiber of 1 m to a vertical resolution of about 5 mm. The high-resolution temperature profiler was tested at a losing reach of the Swiss prealpine River Thur resulting in a 20-day long temperature time series with a temporal resolution of 10 min. The time series are analyzed by means of dynamic harmonic regression to obtain the diurnal contributions of the measured time series at all depths and time points. The time for the diurnal temperature signal to reach the observation depth and the associated attenuation of the signal are calculated from the phase angles and amplitudes of the diurnal contributions. The time shift results in an apparent celerity of diurnal temperature propagation, which is converted into an apparent seepage rate by fitting the data to the analytical solution for convective–conductive heat transfer in a semi-infinite, uniform, one-dimensional domain with a sinusoidal surface temperature. The high spatial resolution allows the location of discontinuities in the river bed which would have remained undetected if temperature had been measured only at a few individual depths to be identified. This is a particular strength of the fiber-optic high-resolution temperature profiler. The time series also give evidence of sporadic high infiltration rates at times of high water tables.

© 2009 Elsevier B.V. All rights reserved.

Introduction

River–groundwater interactions

The transition zone between surface water bodies and groundwater is known as the hyporheic zone. In recent years, this zone has been identified as crucial for the ecological status of the open-water body and the quality of groundwater. The hyporheic zone acts as habitat for benthic organisms playing an important role in river ecology. Furthermore, transformations of nutrients (Brunke and Gonser, 1997; Triska et al., 1993) and pollutants (Bosma et al., 1996; Schwarzenbach and Westall, 1981) occur within the hyporheic zone. For the assessment of groundwater quality in the vicinity of losing rivers, it is of particular importance to know how fast river water infiltrates into the underlying aquifer.

The exchange processes between surface water and groundwater vary both in time and space (Brunke and Gonser, 1997; Huggenberger et al., 1996; Woessner, 2000). Temporal fluctuations may be caused by asynchronous water-table fluctuations in the river and the aquifer (Wroblicky et al., 1998), whereas the reasons for spatial variations lie in the heterogeneity of streambed sediments and associated hydraulic conductivity (Fleckenstein et al., 2006; Huggenberger et al., 1996; Kalbus et al., 2009), in river morphology and stream curvature (Cardenas et al., 2004; Gooseff et al., 2005; Harvey and Bencala, 1993), and in spatially varying hydraulic gradients (Storey et al., 2003). Clogging layers within the river bed may be formed during continuous low river water level periods, causing a reduction in bank filtration. During floods, the clogging layers may be eroded. Such changes in the hydraulic characteristics of the river bed contribute to the dynamics of hyporheic exchange.

Natural rivers exhibit stronger spatial and temporal dynamics of the river bed than regulated rivers. Current efforts of river restoration are designed to re-establish a more natural sediment regime. This increases the variability and potentially the magnitude of hyporheic-exchange processes, and also affects the associated

* Corresponding author. Tel.: +41 (0) 44 8235298; fax: +41 (0) 44 8235210.

E-mail addresses: tobias.vogt@eawag.ch (T. Vogt), olaf.cirpka@uni-tuebingen.de (O.A. Cirpka).

alluvial aquifer systems. Groundwater management in such contexts requires methods for quantifying the exchange of water and solute mass between surface and subsurface water bodies.

A wide range of methods exist to estimate water flux between surface water and groundwater. Kalbus et al. (2006) have reviewed the most common methods, including direct measurement of water flux (seepage meter), estimates of specific discharge from piezometer data (hydraulic gradient, hydraulic tests), heat-tracer methods (based on vertical streambed temperature profiles), and mass balance approaches (differential discharge gauging, solute tracer methods).

In this paper, we present a new method for measuring highly resolved vertical temperature profiles in surface-water sediments. We wrap an optical fiber around a piezometer tube and measure the temperature distribution along the fiber by means of distributed temperature sensing (DTS) based on Raman scattering. From the travel time and attenuation of the diurnal temperature signal, we can estimate the apparent velocity and diffusivity of temperature propagation, which can then be used to approximate infiltration rates. A particular strength of the new measurement technique lies in the high spatial and temporal resolution, enabling us to detect non-uniformity and temporal changes in vertical water flux. We demonstrate the applicability of the method at a restored river section of the River Thur in Switzerland, which is currently under intensive investigation with respect to hyporheic-exchange processes.

Temperature as a natural tracer

Heat is an easy to measure natural physical parameter. The vertical and lateral temperature distribution is a function of boundary conditions, heat conduction and convection (Anderson, 2005; Bredehoeft and Papadopulos, 1965; Lapham, 1989; Stallman, 1965; Suzuki, 1960). Streambed temperature profiles have been used to identify losing and gaining reaches of rivers (Constantz, 2008; Constantz and Stonestrom, 2003; Silliman and Booth, 1993). Conant (2004) as well as Schmidt et al. (2007) obtained spatial patterns of groundwater exfiltration using temperature and piezometer data from a dense monitoring network. They analyzed snapshots of vertical temperature profiles with a model assuming steady-state heat transfer. The applicability of this model is questionable because river temperatures typically exhibit a diurnal cycle so that the streambed temperature is transient.

Under infiltrating conditions, the steady-state contribution to temperature profiles cannot be used for the quantification of seepage rates. However, time series obtained at several depths contain information on both effective convection and conduction in the sediment. Because diurnal temperature variations are periodic and more or less sinusoidal, Stallman's (1965) analytical expression of the convection-conduction equation for sinusoidal boundary conditions is a good starting point for the analysis of temperature data. Hatch et al. (2006) applied a band-pass filter to pairs of temperature time series obtained at different depths within the sediment. Mean flow rates were estimated from the amplitude and phase angle determined for each day using a semi-automated computer program. Kerry et al. (2007) extracted sinusoidal components with periods of one day from temperature time series at various depths using DHR (Young et al., 1999). In this approach, the amplitude and phase angle were estimated as continuous, auto-correlated time variables. Following the analysis of amplitude and phase-angle information of Stallman (1965), Kerry et al. (2007) obtained the seepage rate as a continuous time variable rather than as a set of daily values.

Fiber-optic distributed temperature sensing

Traditional temperature sensors, such as thermocouples and platinum resistance thermometers, measure temperatures only at

individual points. In order to obtain spatial profiles one may either install a large number of individual sensors, or a single sensor is moved along the profile, leading to an asynchronous measurement. An alternative to traditional thermometry is fiber-optic distributed temperature sensing (DTS), which has recently been applied in hydrological studies (Selker et al., 2006a; Tyler et al., 2009). In DTS, temperature is measured along an optical fiber of up to several km in length with a spatial resolution of about 1 m. Thus, thousands of traditional thermometers are replaced by a single fiber. Depending on the required accuracy, the temporal resolution is in the order of several minutes. Thus DTS is an attractive method to obtain long profiles of temperatures that vary on time scales of hours and longer.

DTS is based on the temperature dependence of Raman scattering (Dakin et al., 1985; Kurashima et al., 1990). Light from a laser pulse is scattered along the optical fiber. In addition to standard Rayleigh scattering, in which the frequencies of the original and scattered light are identical, secondary maxima with shifted wavelengths exist. Raman scattering describes a particular pair of secondary maxima. The scattered light with longer wavelength (Stokes) is not affected by temperature, whereas the amplitude of the scattered light with shorter wavelength (anti-Stokes) depends exponentially on temperature of the fiber at the scattering point. The back-scattered light is detected in the DTS control unit with high temporal resolution. The distance to the point where the scattering occurred is the time since the pulse was released times the speed of light, whereas the ratio of the Stokes to Anti-Stokes signals is informative about the temperature at the scattering point. By sampling the responses to multiple pulses with a high temporal resolution, the temperature along the fiber can be measured with high accuracy and high spatial resolution. A more detailed overview of the technique is given by Selker et al. (2006a). Tyler et al. (2009) summarized calibration, operation, limitations, and system accuracies of DTS for hydrological purposes.

The use of DTS in hydrological systems has been mainly focused on lateral measurements at the surface water-groundwater interface. Optical fibers have been laid out laterally to detect submarine groundwater discharge (Henderson et al., 2008), to identify groundwater discharge zones in streams (Lowry et al., 2007; Selker et al., 2006b) and to calibrate an energy-based stream temperature model with DTS data (Westhoff et al., 2007). A limitation of lateral DTS data is that groundwater discharge or recharge rates cannot directly be quantified. If groundwater temperatures differ from river temperatures, local exfiltration of groundwater leads to a local change of the temperature at the river bottom. However, the quantitative relationship between specific discharge and observed temperature is strongly affected by river velocities and vertical mixing within the river. Also, infiltration of river water has essentially no effect on the temperature at the river bottom.

Vertical temperature profiles in boreholes were obtained by DTS for the first time in the 1990s (Hurtig et al., 1994). The application in deep boreholes is simple because the optic fiber only has to be lowered down the borehole. For investigation of near-surface processes, we require a high spatial resolution of temperature. Because the spatial resolution of DTS along the fiber is in the range of 1 m, a straight cable in a shallow borehole will not give the required resolution. A second potential shortcoming of such a set-up lies in the danger of vertical convection in the open or fully screened borehole. To overcome these deficiencies, we adopted the technique of wrapping the optical fiber around a pole or tube, developed by Selker et al. (2006a) in the application of temperature monitoring in lakes and snow fields. Rather than inserting this profiler into an existing piezometer, we wrapped the fiber directly around a new piezometer tube which we install in the subsurface by a dual-tube direct-push technique. The temperature profile along the fiber is converted into a depth profile. The set of time ser-

ies is analyzed by means of dynamic harmonic regression (Keery et al., 2007; Young et al., 1999).

Theory

Convection–conduction equation with sinusoidal boundary condition

We assume that horizontal variability of the seepage process and the related heat transport can be neglected, so that only the vertical component of flow and heat transfer need to be considered. We also consider local thermal equilibrium between groundwater and sediment matrix. Then, the heat transfer from the river into the aquifer can be described by the one-dimensional convection–conduction equation (modified after Anderson (2005) and Stallman (1965)):

$$(\rho_s C_s (1-n) + \rho_w C_w n) \frac{\partial T}{\partial t} + \rho_w C_w q \frac{\partial T}{\partial z} - (\lambda_s (1-n) + (\lambda_w + \rho_w C_w D_{disp}) n) \frac{\partial^2 T}{\partial z^2} = 0 \quad (1)$$

in which we have assumed uniform coefficients. ρ_w , C_w , and λ_w are the mass density (kg/m³), specific heat capacity (J/kg/K), and heat conductivity (W/m/K) of water. ρ_s , C_s , and λ_s are the corresponding properties of the solids; n denotes porosity, q is the vertical component of the specific discharge vector, D_{disp} is the hydrodynamic dispersion coefficient, t is time, and z is the vertical coordinate (positive downwards). The first term in Eq. (1) quantifies the storage of heat per bulk volume in the solid and aqueous phases, the second term expresses the divergence of the vertical convective heat flux caused by the specific discharge of water, whereas the third term denotes the divergence of the bulk conductive heat flux including conduction in the aqueous and solid phases as well as heat dispersion caused by unresolved variations of convection. By dividing Eq. (1) with the term preceding the rate of change of temperature and aggregating terms, the convection–conduction equation may be rewritten as:

$$\frac{\partial T}{\partial t} + v_T \frac{\partial T}{\partial z} - D_T \frac{\partial^2 T}{\partial z^2} = 0 \quad (2)$$

which is the advection–dispersion equation applied to temperature with the effective velocity v_T and effective diffusivity D_T of temperature transport:

$$v_T = \frac{\rho_w C_w}{\rho_s C_s (1-n) + \rho_w C_w n} q; \quad D_T = \frac{\lambda_s (1-n) + (\lambda_w + \rho_w C_w D_{disp}) n}{\rho_s C_s (1-n) + \rho_w C_w n} \quad (3)$$

As boundary conditions, we consider a fixed temperature at the bottom of the stream, $z = 0$, with periodic fluctuations, and vanishing fluctuations at the limit $z \rightarrow \infty$:

$$T(z=0, t) = \bar{T}_0 + a_0 \times \cos(2\pi(t - t_0^{\max})f) \quad (4)$$

$$\lim_{z \rightarrow \infty} T(z, t) = \bar{T}_\infty$$

in which \bar{T}_0 and \bar{T}_∞ are the mean temperatures in the river and the aquifer at infinite distance from the stream bottom, respectively, a_0 is the amplitude of temperature fluctuations in the river, f is the frequency, and t_0^{\max} is the time of maximum temperature in the river.

The analytical solution for heat transfer in the aquifer with sinusoidal surface temperature can easily be determined by spectral analysis (Stallman, 1965):

$$T(z, t) = \bar{T}_0 + a_0 \times \exp\left(-\frac{z}{z_p}\right) \times \cos\left(2\pi\left(t - t_0^{\max} - \frac{z}{c}\right)f\right) \quad (5)$$

in which c and z_p are the frequency-dependent celerity and penetration depth of temperature propagation, respectively.

$$c = v_T \sqrt{\frac{1}{2} + \frac{1}{2} \sqrt{1 + \frac{64\pi^2 f^2 D_T^2}{v_T^4}}} \quad (6)$$

$$z_p = \frac{2D_T}{c - v_T} \quad (7)$$

Eqs. (5)–(7) state that, under steady-state flow conditions, periodic temperature signals of the river are propagated linearly into the aquifer. The celerity c is somewhat higher than the effective velocity v_T of convective temperature transfer. The acceleration in comparison to v_T is higher for higher values of fD_T/v_T^2 . The propagated temperature fluctuation is dampened according to an exponential law. Higher effective diffusivity values D_T for temperature and higher frequencies increase the strength of dampening.

As mentioned above, we assume that sediments and groundwater are in local thermal equilibrium. This assumption can be tested by computing the characteristic time $\tau_{\text{cond}}^{\text{grain}}$ of conductive heat transfer into a spherical grain (modified after vanGenuchten (1985)):

$$\tau_{\text{cond}}^{\text{grain}} = \frac{r^2 \rho_s C_s}{9\lambda_s} \approx r^2 \times 9.1 \times 10^4 \frac{\text{s}}{\text{m}^2} \quad (8)$$

in which r is the grain radius. For a typical grain diameter of 2 cm, the time $\tau_{\text{cond}}^{\text{grain}}$ to heat up the grain is approximately 9 s, which is considerably smaller than the period of diurnal temperature fluctuations.

A second crucial assumption is that of uniform coefficients. Analyzing a specific spectral component with specific frequency f , the latter condition can be relaxed: for $z \gg z_p(f, D_T, v_T)$, a change in D_T or v_T has only a negligible effect on the solution. In particular, this implies that the steady-state contribution $\bar{T}(z)$ may be affected by a boundary condition or change in coefficients at some depth z , whereas the diurnal signal may not be influenced because $z_p(f) \ll z$.

Dynamic harmonic regression

As discussed in detail below, we measure time series of temperature at multiple depths in the streambed using distributed temperature sensing. Like Kerry et al. (2007), we use the dynamic harmonic regression technique of Young et al. (1999) to obtain the diurnal signal from the measured time series of temperature. For DHR, we use the Matlab-based captain toolbox (Young et al., 2007) developed at Lancaster University. The forward model is similar to the standard spectral representation of the time series:

$$T(t) = a_0(t) + \sum_{i=1}^{n_f} \left(\alpha_i(t) \cos\left(2\pi i \frac{t}{\tau}\right) + \beta_i(t) \sin\left(2\pi i \frac{t}{\tau}\right) \right) \quad (9)$$

in which $a_0(t)$ is the trend, whereas $\alpha_i(t)$ and $\beta_i(t)$ are the sine and cosine contributions of the frequency i/τ , in which τ is the base period (here one day). In contrast to standard Fourier transformation, the spectral coefficients $a_0(t)$, $\alpha_i(t)$, and $\beta_i(t)$ themselves are time-dependent variables. That is, DHR is a non-stationary extension to Fourier analysis. The coefficients $a_0(t)$, $\alpha_i(t)$, and $\beta_i(t)$ are considered stochastic, time variable parameters: Both the absolute values and the time derivatives of the individual coefficients are correlated in time. The evaluation of the coefficients involves forward pass filtering, smoothing, and backward pass filtering, whereas the stochastic hyper-parameters, expressing the degree of temporal correlation, are estimated by the pseudo-spectral approach of Young et al. (1999). It may be worth noting that determining optimal hyper-parameters is crucial for the analysis. If the temporal auto-correlation of the chosen parameters is too weak, the coefficients vary too strongly, and it becomes impossible to detect a trend of the coeffi-

cients. Conversely, if the temporal auto-correlation is too strong, the variability of the signal remains unrecognized.

From the sine and cosine coefficients, it is straightforward to compute the time-dependent amplitude $a_i(t)$ and phase angle $\varphi_i(t)$ for frequency i/τ at time t :

$$a_i(t) = \sqrt{\alpha_i^2(t) + \beta_i^2(t)} \quad (10)$$

$$\varphi_i(t) = \tan^{-1} \left(\frac{\alpha_i(t)}{\beta_i(t)} \right) \quad (11)$$

We perform DHR to temperature time series obtained at multiple depth z , considering the diurnal base frequency $f = 1/\tau = 1/d$ and the first three harmonics, $f = [2/\tau, 3/\tau, 4/\tau]$. In our application, we estimate the optimal hyper-parameters for a single temperature time series, namely that at the stream–aquifer interface, $z = 0$, and use these hyper-parameters for DHR of the temperature time series at all depths.

Interpretation of dynamic harmonic regression results

The outcome of the dynamic harmonic regression analysis is a set of amplitudes $a(z,t,f)$ and phase angles $\varphi(z,t,f)$ for each time point t , measurement depth z , and analyzed frequency f . For further analysis, we consider only the diurnal signal, $f = 1/d$. In a first step, the phase angle is converted to a time point of maximum temperature t^{\max} :

$$t^{\max}(z,t,f) = -\frac{\varphi(z,t,f)}{2\pi f} \quad (12)$$

It may be worth noting that $t^{\max}(z,t,f)$ is a continuous function in time because the phase angle $\varphi(z,t,f)$ is estimated as continuous time function. In contrast, the true temperature signal typically exhibits only a single time point of maximum temperature per day.

In a second step, we evaluate the time $t_{\text{shift}}(z,t,f)$ needed for temperature propagation from the stream–aquifer interface to depth z at each time point t . For the right value of $t_{\text{shift}}(z,t,f)$, the following identity must hold:

$$t_{\text{shift}}(z,t,f) = t^{\max}(z,t,f) - t^{\max}(0,t - t_{\text{shift}}(z,t,f),f) \quad (13)$$

which requires an iterative evaluation scheme, because the right-hand side involves the estimated time shift $t_{\text{shift}}(z,t,f)$ itself.

For given time shifts $t_{\text{shift}}(z,t,f)$, we can evaluate which attenuation $A(z,t,f)$ the diurnal temperature signal, or any other periodic contribution, has undergone during its propagation from the surface to depth z at each time point t :

$$A(z,t,f) = \ln \left(\frac{a(0,t - t_{\text{shift}}(z,t,f),f)}{a(z,t,f)} \right). \quad (14)$$

Likewise, we can compute the apparent celerity $c(z,t,f)$ of the temperature signal with frequency f , reaching depth z at time t :

$$c(z,t,f) = \frac{z}{t_{\text{shift}}(z,t,f)} \quad (15)$$

From the apparent celerity $c(z,t,f)$ and the attenuation $A(z,t,f)$, we may evaluate apparent values of the effective velocity $v_T(z,t,f)$ and effective diffusivity $D_T(z,t,f)$ of temperature transport by minimizing the sum of squared relative residuals of $c(v_T, D_T, f)$ and $z_p(v_T, D_T, f)$ according to Eqs. (5)–(7):

$$W(v_T, D_T) = \left(1 - \frac{v_T}{c} \sqrt{\frac{1}{2} + \frac{1}{2} \sqrt{1 + \frac{64\pi^2 f^2 D_T^2}{v_T^4}}} \right)^2 + \left(1 - \frac{2AD_T}{(c - v_T)z} \right)^2 \quad (16)$$

in which we have dropped the argument (z, t, f) for convenience, and c as well A are the values derived from the analysis of DHR. Optimization is done by the Nelder–Mead simplex algorithm as implemented in the Matlab function `fminsearch` (Lagarias et al., 1998).

Finally, we estimate an apparent seepage rate $q(z,t)$ from the apparent velocity $v_T(z,t,f)$ of temperature transport related to the diurnal signal, $f = 1/d$:

$$q(z,t) = v_T(z,t,f) \frac{\rho_s C_s (1-n) + \rho_w C_w n}{\rho_w C_w} \quad (17)$$

for which we need an estimate of the porosity n .

The term “apparent” used above relates to the interpretation of parameters obtained from a process varying in time and space as if caused by a process with uniform coefficients. The apparent velocity $v_T(z,t,f)$ is the path averaged effective velocity of temperature transport, at best.

Experimental set-up

Fiber-optic vertical temperature profiler

The fiber-optic vertical temperature profiler consists of a solid 2 in. PVC piezometer tube (OD = 50.8 mm) of 2 m length and an optical fiber (Fig. 1). We wrap 380 m of the optical fiber (OD = 0.9 mm) around the tube (OD = 60 mm) using a lathe. This converts the spatial resolution of the DTS from 1 m along the optical fiber to a vertical resolution of 4.9 mm along the 1.86 m long wrapped tube section. The optical fiber is protected against mechanical damage by covering it with a self-adhesive plastic film. The total diameter (PVC piezometer tube + 2 fibers + plastic film) is about 63 mm. At the lower end, the PVC piezometer tube has a female connector. Here, the outer diameter of the PVC tube increases to 65 mm, and the tube is not wrapped. The lower end of the tube is closed with a plug. Small holes permit hydraulic head measurements at the bottom of the profiler. The optical fiber is led through one of these holes to the inside of the tube and runs back to the top, which allows dual-ended DTS measurements.

The PVC wrapped piezometer tube fits into the 3.25 in. rods (OD = 82.5 mm, ID = 67 mm) of the Geoprobe® direct-push system. For installation, we push 3.25 in. rods with an expandable tip into the river bed using a Geoprobe® 6620DT machine. The wrapped piezometer tube is inserted into the 3.25 in. rods, and the outer rods are extracted, leaving the tip and the wrapped piezometer tube in the sediments. Subsequently, the delicate optical fibers are spliced to a standard outdoor fiber-optic communication cable. The communication cable is led through a cap screwed onto the male thread at the upper end of the PVC piezometer tube. The stress-resistant outdoor communication cable connects the fiber-optic vertical temperature profiler with the DTS control unit.

The optical fiber used for wrapping (Dätwyler GF-100) has a multi-mode glass core, 0.05 mm thick, with a critical bending radius of 25 mm. Although the latter would allow using a tube with smaller diameter, we prefer 2 in. PVC piezometer tubes to minimize signal loss in the wrapped fiber section and to achieve a high vertical resolution. We calibrated the fiber-optic vertical temperature profiler in the laboratory with two reference sections at two known temperatures.

We used an Agilent N4386 DTS system to measure the temperature along the fiber operating with 1 m sampling interval, 1.5 m spatial resolution and single-ended measurements averaged over 10 min. The theoretical temperature resolution is 0.11 K for a 2 km long fiber, 10 min integration time, and 1.5 m spatial resolution in single ended measuring mode (according to technical data-sheet of manufacturer, AP Sensing GmbH, 2009). We selected a

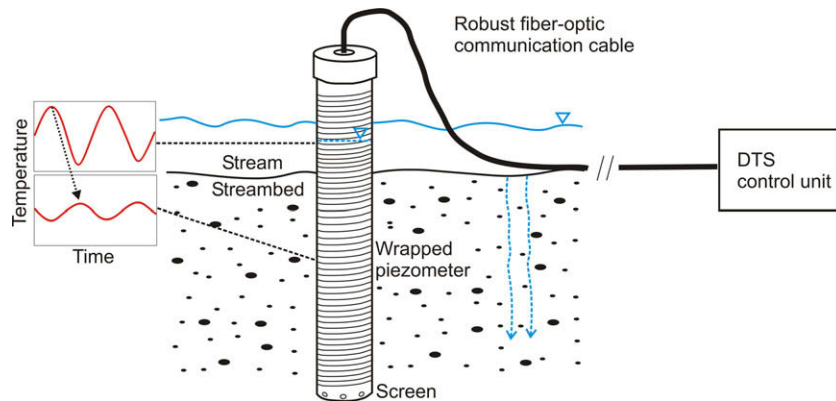


Fig. 1. Schematic outline of the fiber-optic high-resolution vertical temperature profiler.

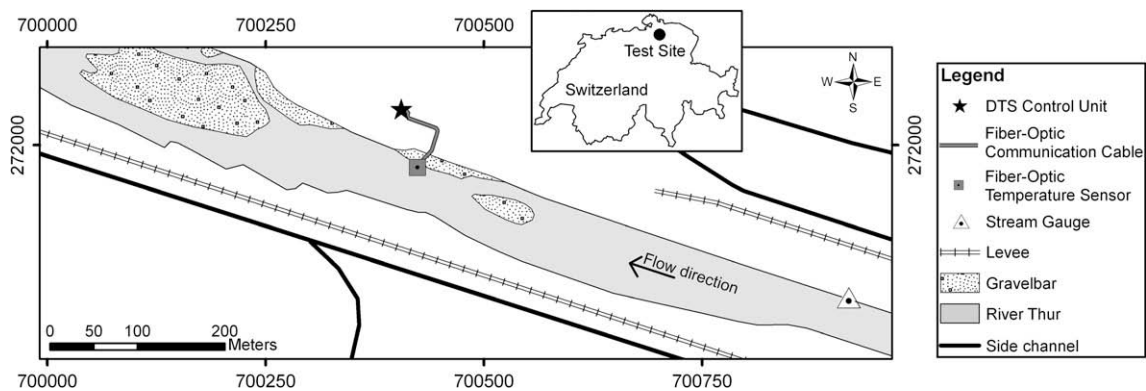


Fig. 2. Location of the test site at a restored section of Swiss River Thur in Niederneunforn, Canton of Thurgau. Easting and northing in Swiss coordinates.

sampling interval of 1 m to obtain highest vertical resolution, although the temperature resolution is degraded with small sampling intervals (<3 m). Hence, we chose a measurement time of 10 min to assure a proper temperature resolution. Decreasing measurement time may yield higher temporal resolution, but would provide little practical benefit because of the diurnal character of temperature oscillations.

Field site

We test our fiber-optic vertical temperature profiler at a restored section of River Thur, a tributary to River Rhine in North-East Switzerland. River Thur is the largest Swiss river (total length of 127 km; catchment area of about 1750 km²) without a natural or artificial lake along its course and exhibits fluctuations in discharge and water table similar to unregulated Alpine rivers (low discharge: 3 m³/s; mean discharge: 20–50 m³/s; peaks up to 1000 m³/s; Federal Office for the Environment, <http://www.bafu.admin.ch/publikationen/01005>). Snowmelt and strong rain events in the prealpine headwaters, with Mount Säntis (2502 m a.s.l.) being the highest point, cause short but rapid increase of discharge. Mean annual precipitation of the field site area is 908 mm and average monthly temperature ranges from 0.9 °C in January to 19.0 °C in July (<http://gate.meteoswiss.ch/idaweb>).

The geology of the Thur aquifer is dominated by glacio-fluvial sandy gravels overlaying lacustrine clays. The gravel deposition occurred within a couple of thousand years at the end of the last ice age during the retreat of the last Rhine glacier. In some parts of the valley, natural alluvial fines of up to 2 m thickness act as a hydraulic barrier between ground surface and gravel aquifer. This confin-

ing layer is absent at the location where the fiber-optic vertical temperature profiler was installed.

The research site is located in Niederneunforn, Canton Thurgau (Fig. 2). Here, the overbanks have been removed over a length of approximately 2.5 km. The width of the losing river is about 100 m. The principle direction of groundwater flow on this site of the river is from the river towards a side channel in 180 m distance. At the location of installation, the river cuts into sandy gravel sediments. The thickness of the gravel layer is about 6 m with an average hydraulic conductivity of 5×10^{-3} m/s (variance: $\sigma_{\log k}^2 = 0.4$ (Amt für Umwelt Kanton Thurgau, 2008)). The clay below the gravel can be addressed as impervious.

As illustrated in Fig. 3, the fiber-optic vertical temperature profiler has been installed on the North side of the river bed (northing: 271'974, easting: 700'423 in Swiss coordinates, level of the river bed surface: 371.5 m a.s.l.). The screen-point with the lower end of the wrapped fiber was situated 1.45 m below the sediment surface. Due to the vertical resolution of 4.9 mm of the probe, 296 measuring points recorded temperature variation within the sediments. A combined water-level and temperature sensor (STS DL/N 70), located 520 m upstream of the measuring point, measured the river stage and water temperature every 15 min. The data presented here were obtained during 20 days in May–June 2008.

Results

Distribution of temperature in time and depth

Fig. 4 shows the spatiotemporal distribution of temperature along the fiber-optic vertical temperature profiler. The part of the temperature profiler above the river bed measured the tempera-



Fig. 3. Photograph of the site showing direct-push installation of the fiber-optic vertical temperature profiler. Viewing direction is downstream.

tures of river water and air. Fig. 4A shows the time series of these data as lines. The data of the river temperature logger agree well with the DTS measurements over the monitored period. Deviations occur due to calibration and signal noise of the DTS as well as solar radiation that maybe heats up the shallow water at the bank or directly the cable in the river water during the period from 23rd to 26th of May because river stage was very low. During the stream-bed temperature profiling in May–June 2008, river water temperatures varied diurnally, reaching a minimum value of 7.2 °C and a maximum of 24.8 °C (Fig. 4A). From 17th to 23rd of May, the river stage rose and the temperature amplitudes decreased. The river gauge data (blue line in Fig. 4B) show very close agreement with the river stage estimated from the DTS data.

The high resolution of the fiber-optic vertical temperature profiler gives a detailed view of the variation of river bed temperature over depth and time. Fig. 4B shows a general trend of decreasing temperature with depth but an overall increase over the period under investigation starting on 23rd of May indicating heating up of the deeper aquifer over seasonal time scales. In the following analysis only the diurnal fluctuations are considered. Visual inspection of Fig. 4B shows that the amplitude of temperature oscillations is damped with depth. Also, small time shifts with depth in the occurrence of the maximum temperature are visible. At a certain depth the temperature fluctuations are strongly damped and eventually become non-detectable. The zone of strong damping starts at 0.6 m depth. A particular strength of the fiber-optic vertical temperature profiler lies in the detection of such zones and their variability. In contrast, DTS data at the top and bottom of the wrapped piezometer show spurious temperature anomalies caused by high signal noise and fiber properties at the beginning and end of the fiber (see horizontal stripes in Fig. 4B). This kind of measurement error is common for DTS data and can partially be attributed to the instrument's sampling resolution/spatial resolution algorithm (Tyler et al., 2009).

Results of dynamic harmonic regression analysis

As described in Sections “Dynamic harmonic regression” and “Interpretation of dynamic harmonic regression results”, we apply dynamic harmonic regression to the temperature time series of

each depth z . The time series at $z = 0$ acts as river-water reference. Regular inspection of the test site confirmed that no erosion or sedimentation occurred throughout the period monitored. Thus, depth is known and constant over time. Due to the bad signal-to-noise ratio and the temperature resolution of the DTS system used, we do not analyze temperatures recorded deeper than 1.2 m. Fig. 5 shows the results of DHR analysis for the frequency $f = 1/d$. Fig. 5A illustrates the estimated amplitudes of the diurnal temperature oscillations, whereas Fig. 5B shows the times at which the estimated diurnal temperature oscillation has its amplitude. The latter is estimated by unwrapping the phase angle (Eq. (12)). Times larger than 24 h reflect the fact that the maximum occurs on the next day.

The amplitudes and times of the diurnal temperature maximum shown in Fig. 5 reflect characteristics of temperature transport in the subsurface. Amplitudes vary over time and decrease to almost 0 at 1.2 m depth. In the period from 18th to 23rd of May, the water table was higher and the diurnal temperature fluctuations in the river were smaller than in the preceding and following times, reflecting the weather conditions during this period, with 16.3 mm precipitation from 17th to 19th of May. During this time period, the temperature amplitudes are also smaller in the subsurface, and they are less dampened.

At shallow depths, down to 0.6 m, the time of maximum temperature increases almost linearly. Between 0.6 and 0.8 m depth, temperature maxima are propagated much more slowly, which is indicated by a strong increase in the time of maximum temperature with depth. Below 1 m depth, the noise in the DTS signal caused anomalies in the times of maximum temperature, especially towards the end of the monitoring campaign.

Evaluation of apparent parameters of heat transfer

From the time of maximum temperature, shown in Fig. 5B, we evaluate the time shift of the diurnal temperature signal by Eq. (13). The resulting spatiotemporal distribution is shown in Fig. 6A, whereas Fig. 6B shows the attenuation of the diurnal temperature signal according to Eq. (14). At shallow depths, the time shifts increase more or less linearly with depth, reaching a value of approximately 3 h at 0.6 m depth. Below 0.6 m depth, the time shift increases much more with depth, indicating slower propaga-

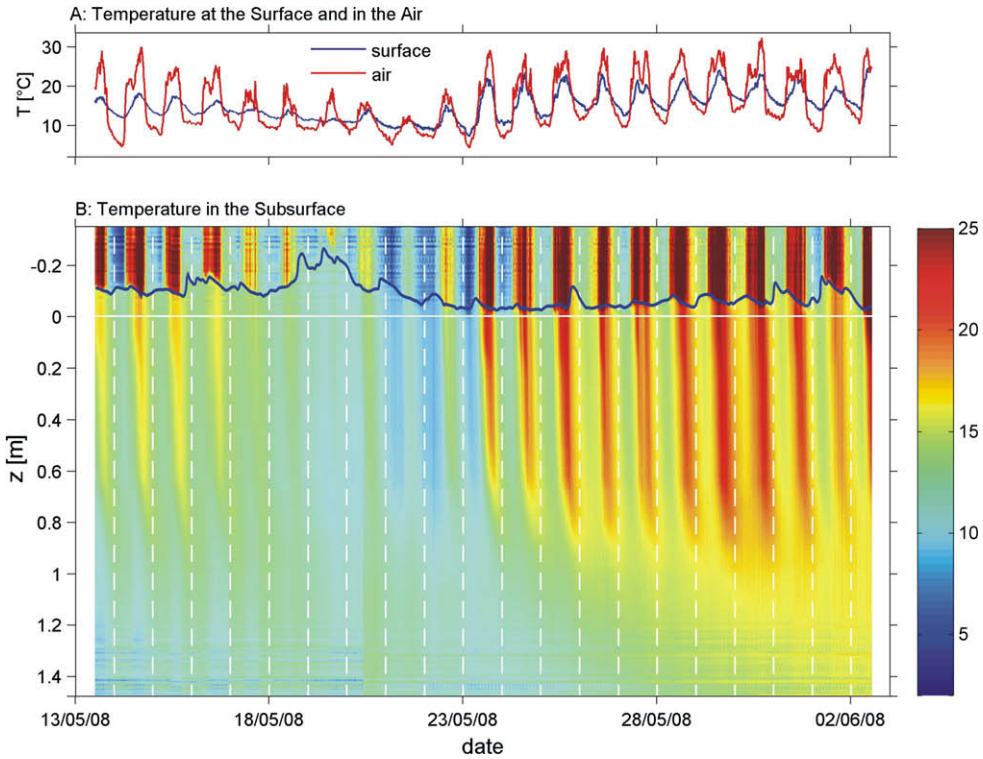


Fig. 4. Spatiotemporal distribution of temperature along the fiber-optic vertical temperature profiler. (A) Surface and air temperature, (B) high-resolution temperature distribution in the subsurface. The blue line indicates the river stage. (For interpretation of the references to color in this figure legend, the reader is referred to the web version of this article.)

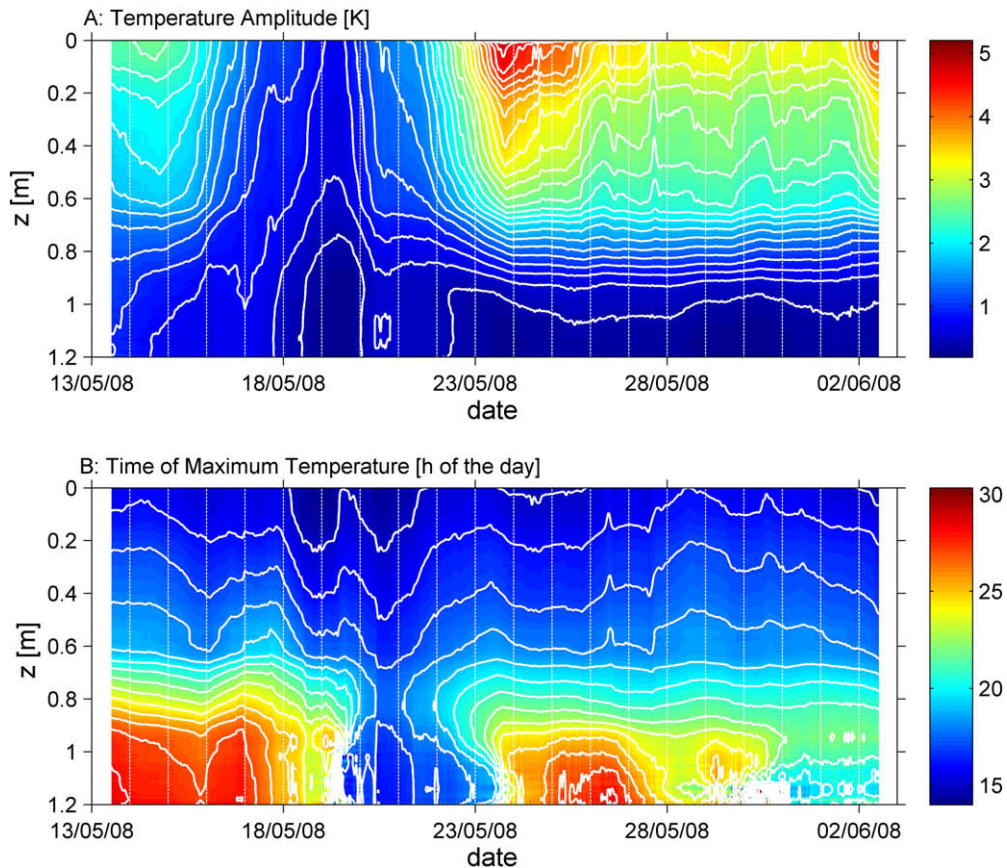


Fig. 5. Temperature amplitude and time of maximum temperature of the diurnal signal according to dynamic harmonic regression. (A) Temperature amplitude with isotherms of 0.2 K. (B) time point of maximum temperature. Contourlines: isochrones of 1 h.

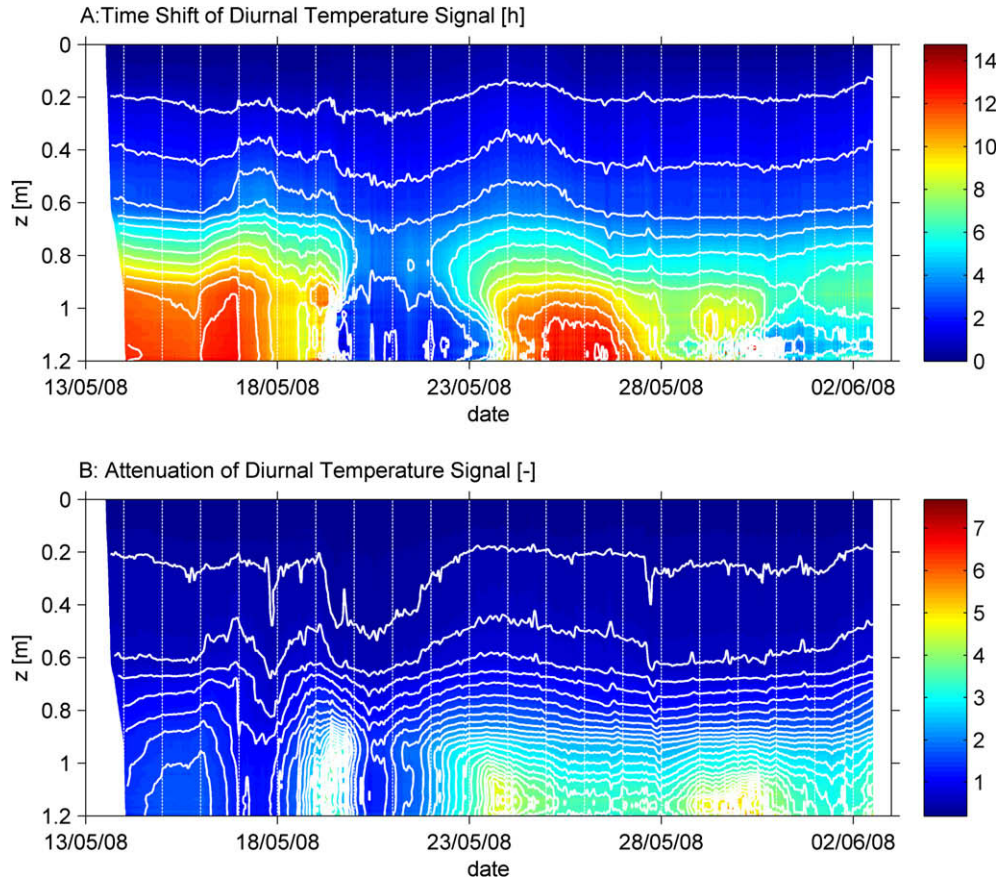


Fig. 6. Interpretation of dynamic harmonic regression results. (A) Time shift of diurnal temperature signal. Contourlines: isochrones of 1 h. (B) attenuation of diurnal temperature signal. Contourlines: isolines of 0.2.

tion of the temperature signals. The difference between the shallow river bed (down to 0.6 m depth) and the somewhat deeper subsurface is also evident in the attenuation of the diurnal temperature signal, which is more pronounced with depth (see Fig. 6B). At the time of higher river stage from 20th to 22nd of May, the attenuation is much smaller, whereas it becomes particularly pronounced with depth in the warm period afterwards.

Solving Eqs. (16) and (17) for each time and depth yields high-resolution apparent seepage rates. The iterative calculation of the apparent velocity was efficient and yielded reasonable values. By contrast, the determination of thermal diffusivity was delicate. Thermal diffusivities evaluated from the attenuation of the diurnal temperature signals ranged between 10^{-8} and 10^{-9} m²/s. If we estimate D_T by Eq. (3) using typical physical thermal properties of sediments (listed in Table 1) and setting D_{disp} to zero, we obtain a value of 6.7×10^{-7} m²/s, which is two orders of magnitude larger than the values evaluated from the attenuation of the diurnal temperature signal. Accounting for dispersion can lead only to a further increase of D_T . Therefore, we opted against fitting the thermal diffusivity from the data, and fixed the value to 6.7×10^{-7} m²/s instead in the remaining evaluation of the effective velocity v_T from the calculated time shifts of the diurnal temperature signals. Results for the estimated v_T values are not shown since they are proportional to apparent seepage rates discussed below.

Apparent seepage rates

We estimate apparent seepage rates q from the effective velocities v_T by Eq. (16). The thermal properties used for calculations are

Table 1

Values for physical properties after Schön (1998) that are used in calculations of effective velocities and thermal diffusivity. The sediment consists of a quartz–calcite mixture. The porosity is estimated.

	Density (kg/m ³)	Specific heat capacity (J/kg/K)	Heat conductivity (W/m/K)	Porosity
Water	1000	4185	0.58	
Solids	2680	733	2.4	0.25

listed in Table 1. The river bed sediment is sandy gravel consisting mainly of quartz and calcite determined by core soundings. In contrast to hydraulic properties, thermal sediment properties have a narrow range. Hence, the uncertainty of flux calculations caused by variability of the thermal properties is not significant (Keery et al., 2007).

Fig. 7 shows the seepage rates evaluated from v_T by Eq. (16) compared to the river stage. Due to unreasonable fluctuations close to the surface and below 1.1 m depth, we show estimated apparent seepage rates from only 0.1–1.1 m depth. The sediments at the surface are disturbed during the installation of the temperature profiler, yielding seepage flux which is too high. Furthermore, the time shifts of diurnal temperature propagation at these shallow depths are very small so that the estimates of v_T are very sensitive to small errors. The temperature resolution of the DTS system used affects the calculated seepage rates only at deeper depths, especially where amplitudes are below 0.1 K and cannot be resolved with the DTS system. The values at depths larger than 1.1 m are also affected by the small signal-to-noise ratio on the temperature records.

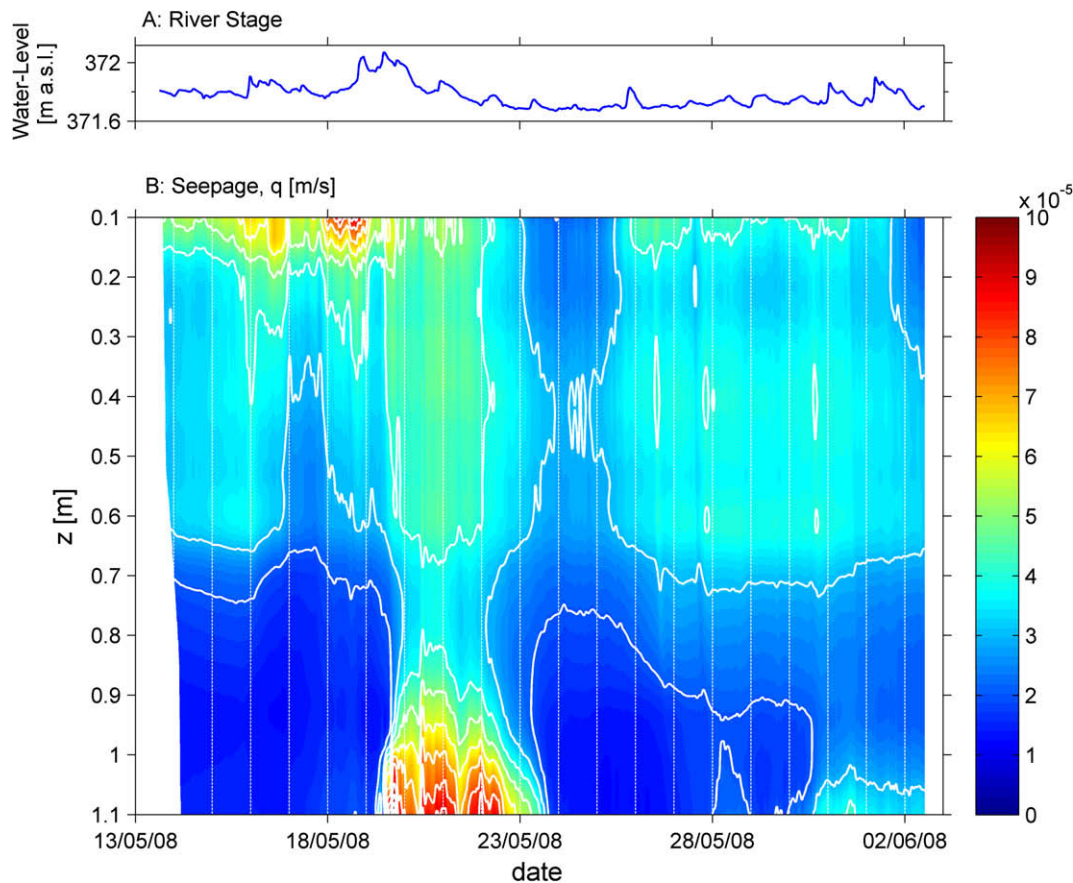


Fig. 7. Estimated apparent seepage fluxes compared to the river stage. (A) River stage of gauging station. (B) Calculated vertical seepage fluxes. Contourlines: isolines of 1×10^{-5} m/s.

Over the entire observation period shallow depths exhibit stronger apparent fluxes ($3.0\text{--}4.0 \times 10^{-5}$ m/s) than depths below 0.6 m ($1.5\text{--}2.5 \times 10^{-5}$ m/s). To demonstrate the depth dependency of the estimated seepage flux, Fig. 8A shows calculated values at three different depths as a function of time. While the values at 0.4 and 0.6 m depth are consistent, the value at 0.8 m is significantly smaller.

The estimated apparent seepage fluxes vary also over time (see Fig. 7B and Fig. 8A). The highest infiltration occurred between 20th and 22nd May during falling river stage after a small event (see greenish and reddish color¹ in Fig. 7B during this period). The small temperature amplitudes during this time at a depth below 0.9 m may have distorted the estimate of seepage rates (see also the profile of the apparent seepage rate on 20th of May in Fig. 8B). However, it is also possible that during this event the flow paths differed so that the comparably warm water at depth on 20th May was laterally transported to the profiler. From 26th May, the estimated seepage rates stabilize, which is in agreement with only small fluctuations in river stage.

Comparison to hydraulic conductivity measurements

In the process of installing the fiber-optic vertical temperature profiler, sediment cores were sampled. Unfortunately, these core samples were incomplete because the grain diameter of the gravel was too big for direct-push sediment sampling. To elucidate the vertical variability of hydraulic conductivity, we performed slug

tests at two locations in the vicinity of the fiber-optic temperature profiler at a depth of 0.5 m and 1.0 m. The hydraulic conductivity averages in 0.5 m depth 3.6×10^{-3} m/s and decreases in 1.0 m depth to 2.3×10^{-3} m/s. The average hydraulic gradient for 0.5 m and 1.0 m depth was 0.02, which is identical to that measured at the fiber-optic temperature profiler. Based on Darcy's law the Darcy velocity is 7.2×10^{-5} m/s in 0.5 m depth and 4.6×10^{-5} m/s in 1.0 m depth. The trend to lower velocities below 0.6–0.7 m depth, determined by DTS data, is thus consistent with the slug test outcome. The higher seepage of the Darcy based method results from head measurement error, which is in the range of 0.005 m.

Discussion and conclusions

All techniques for the estimation of seepage fluxes are prone to errors, uncertainties and limitations (Kalbus et al., 2006). Field investigations are often limited by instrumentation and insufficient resolution. But for detailed assessment of spatial heterogeneity and temporal variability of river-groundwater interaction, high-resolution measurements are necessary. The present work builds upon previous studies in which infiltration rates were determined from temperature time series (Constantz and Stonestrom, 2003; Hatch et al., 2006; Keery et al., 2007; Silliman and Booth, 1993). The main innovation of the current contributions lies in achieving high vertical resolution of the temperature measurement by applying distributed temperature sensing to an optical fiber wrapped around a tube that is installed in the river bed. Previous work on time series analysis of streambed temperature data considered only very shallow depths (max. 0.5 m). In these

¹ For interpretation of color in Fig. 7, the reader is referred to the web version of this article.

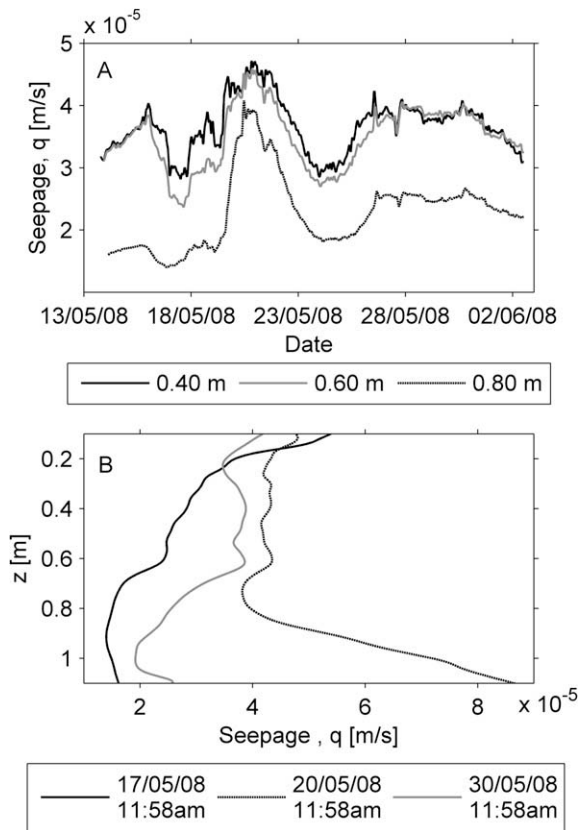


Fig. 8. Spatial and temporal variability of apparent seepage flux. (A) Apparent seepage flux at three depths as function of time. (B) Apparent seepage flux at three times as function of depth.

studies, a small number of thermometers were installed in vertical profiles. As in these previous studies, we analyze streambed temperature data with a model based on the assumption that the vertical seepage rate is constant with depth, even though the data indicate non-uniform vertical flow. This is why the determined coefficients are described as apparent ones.

In principle, the uncertainties in the analysis of temperature time series data are identical for measurements at individual points and for spatially highly resolved measurements along a vertical profile. As analyzed by Keery et al. (2007) and Hatch et al. (2006), among others, neglecting thermal diffusion or attributing a fixed value to D_T as done in our study has only a minor impact on the celerity of temperature propagation under infiltrating conditions in convection-dominated cases. The major uncertainty of quantifying the celerity of temperature propagation is caused by the proper identification of the diurnal temperature signal. The amplitude of diurnal temperature fluctuations must be significantly higher than the accuracy of the temperature sensor. If the seepage flux is constant, retrieval of the diurnal signal is simple and does not even require dynamic harmonic regression (DHR). In highly dynamic cases, separating the diurnal contribution subject to time-varying auto-correlated parameters from the trend contribution, which is also assumed to be auto-correlated, may become delicate. As discussed in Section “Dynamic harmonic regression”, determining optimal hyper-parameters describing the auto-correlation is a crucial step. We have used the pseudo-spectral approach of Young et al. (1999) and inspected some retrieved diurnal signals manually for consistency. This implies the danger of subjective bias of the phase angle $\phi_I(t)$, the time point of maximum temperature t^{\max} , and the time shift $t_{\text{shift}}(z,t)$ according to Eqs. (11)–(13) in cases where the diurnal signal is not very pronounced.

At our site the propagation velocity of temperature varied with depth. In particular, the propagation was faster in the uppermost 0.6 m than below. This depth dependence and the variation of temperature propagation with time are the main experimental findings of the study. It should be noted that the vertical variability would have remained undetected if only two thermometers had been used. That is, the high-resolution measurement was advantageous in detecting vertical variability. While the temporal variation can easily be attributed to changing hydrological conditions, namely the difference between the river stage and the hydraulic head in groundwater at depth, the vertical variation is somewhat more complex.

The analytical expressions that we have fitted to the observed propagation of diurnal temperature signals are based on the assumption of uniform, one-dimensional flow. This is why the estimated seepage rates were denoted apparent ones. Quite obviously, if the apparent velocities differ with travel distance, the underlying assumption of uniformity does not hold. Since apparent velocities are integrated over the travel distance, the variability of local velocities must even be higher.

Vertical variability of hydraulic conductivity alone cannot explain vertical variation of the apparent vertical seepage flux. If the system was truly one-dimensional, continuity would require a uniform vertical flow component no matter how strong the differences in hydraulic conductivity are. A variation of the vertical flux must be balanced by variations of horizontal flux components, requiring spatial variability of the flow field in multiple dimensions. These could be caused by lateral variability of hydraulic conductivity or by boundary conditions, e.g. imposed by the bed form (Cardenas et al., 2004). Obviously, the exact nature of the multi-dimensional flow field cannot be determined by a single vertical profile. This is in accordance with Conant (2004), who demonstrated the variability of seepage rates in a stream. Moreover, Becker et al. (2004) showed that single temperature profile measurements were unrepresentative of overall river–groundwater interaction as measured by heat balance. Therefore, our findings represent only local exchange, but demonstrate that the presented method works. In future studies we thus plan to install a grid of fiber-optic temperature profilers to obtain a multi-dimensional image of the vertical and lateral seepage processes on a larger scale.

The DTS system produces slightly noisy data, particularly in the first and last 15% of the wrapped optical fiber. The spatial and temporal resolution of the DTS system is an important parameter for DTS experiments. As we chose the highest spatial resolution, we used longer sampling times to reduce the impact of temperature resolution on seepage calculations. The high spatiotemporal resolution of the temperature data allowed smoothing, resulting in improved estimates of heat-transport parameters. In our study, performed in sandy gravel, temperature time series in the depth range between 0.1 and 1.1 m could be well analyzed. The top 0.1 m was affected by disturbances potentially caused by the installation, and by the small times of temperature propagation. Below a depth of 1.1 m, the temperature signal was too strongly attenuated, and smaller than the temperature resolution of the DTS system. To which depth diurnal temperature signals are strong enough to allow estimating seepage rates is site specific, and may also vary in time according to changing hydrological conditions. A particular advantage of high-resolution measurements is that the appropriate depth of investigation may be approximated only roughly before installation. If the deeper section of the profiler yields non-analyzable results, the upper section still includes enough measurement points. Also, small changes with time in the vertical temperature profile can easily be detected. This opens up new possibilities for high-resolution vertical temperature monitoring in shallow aquifers, e.g. in the detection of the boundary be-

tween two groundwater bodies differing in their temperature, or in the monitoring of heat-tracer tests. For long term investigations of river water infiltration, the seasonal signal obtained by high-resolution vertical temperature profiles can also be analyzed using the methodology described in this paper with a frequency of 1/y.

Overall, the fiber-optic high-resolution vertical temperature profiler provides high quality temperature data for quantification of river–groundwater exchange. Although this method requires careful design, installation, and calibration, the use of DTS systems for vertical temperature sensing is a promising approach, which may be used for the estimation of seepage rates and beyond.

Acknowledgements

This study was financed by the Competence Center Environment and Sustainability (CCES) of the ETH domain in the framework of the RECORD project (Assessment and Modeling of Coupled Ecological and Hydrological Dynamics in the Restored Corridor of a River (Restored Corridor Dynamics)). We thank Andreas Raffainer and Peter Gäumann of the Eawag workshop as well as Erwin Pieper of the Swiss Federal Institute of Material Research and Testing (Empa) for their help in wrapping the fiber-optic temperature profilers. We are grateful to three anonymous reviewers for their constructive remarks helping to improve the quality of the paper.

References

- Amt für Umwelt Kanton Thurgau, 2008. 2. Thurgauer Thurkorrektur, Abschnitt Weinfelden Bürglen, Szenarienrechnungen. Bericht Simultec AG., unpublished data.
- Anderson, M.P., 2005. Heat as a ground water tracer. *Ground Water* 43 (6), 951–968.
- Becker, M.W., Georgian, T., Ambrose, H., Siniscalchi, J., Fredrick, K., 2004. Estimating flow and flux of ground water discharge using water temperature and velocity. *Journal of Hydrology* 296 (1–4), 221–233.
- Bosma, T.N.P. et al., 1996. Biotransformation of organics in soil columns and an infiltration area. *Ground Water* 34 (1), 49–56.
- Bredhoeft, J.D., Papadopoulos, I.S., 1965. Rates of vertical groundwater movement estimated from earth's thermal profile. *Water Resources Research* 1 (2), 325–328.
- Brunke, M., Gonser, T., 1997. The ecological significance of exchange processes between rivers and groundwater. *Freshwater Biology* 37 (1), 1–33.
- Cardenas, M.B., Wilson, J.L., Zlotnik, V.A., 2004. Impact of heterogeneity, bed forms, and stream curvature on subchannel hyporheic exchange. *Water Resources Research* 40 (8), 14.
- Conant, B., 2004. Delineating and quantifying ground water discharge zones using streambed temperatures. *Ground Water* 42 (2), 243–257.
- Constantz, J., 2008. Heat as a tracer to determine streambed water exchanges. *Water Resources Research*, 44.
- Constantz, J., Stonestrom, D.A., 2003. Heat as a tracer of water movement near streams. In: Stonestrom, D.A., Constantz, J. (Eds.), *Heat as a Tool for Studying the Movement of Ground Water Near Streams*. US Geological Survey, US Geological Survey Circular 1260. US Geological Survey, Reston, VA, pp. 1–6.
- Dakin, J.P., Pratt, D.J., Bibby, G.W., Ross, J.N., 1985. Distributed optical fiber Raman temperature sensor using a semiconductor light-source and detector. *Electronics Letters* 21 (13), 569–570.
- Fleckenstein, J.H., Niswonger, R.G., Fogg, G.E., 2006. River-aquifer interactions, geologic heterogeneity, and low-flow management. *Ground Water* 44 (6), 837–852.
- Gooseff, M.N., Anderson, J.K., Wondzell, S.M., LaNier, J., Haggerty, R., 2005. A modelling study of hyporheic exchange pattern and the sequence, size, and spacing of stream bedforms in mountain stream networks, Oregon, USA (Retracted article. See vol. 20, pp. 2441, 2006). *Hydrological Processes* 19 (15), 2915–2929.
- Harvey, J.W., Bencala, K.E., 1993. The effect of streambed topography on surface–subsurface water exchange in mountain catchments. *Water Resources Research* 29 (1), 89–98.
- Hatch, C.E., Fisher, A.T., Revenaugh, J.S., Constantz, J., Ruehl, C., 2006. Quantifying surface water–groundwater interactions using time series analysis of streambed thermal records: method development. *Water Resources Research* 42 (10), 14.
- Henderson, R.D., Day-Lewis, F.D., Lane Jr., J.W., Harvey, C.F., Liu, L., 2008. Characterizing submarine ground-water discharge using fiber-optic distributed temperature sensing and marine electrical resistivity. In: *Symposium on the Application of Geophysics to Engineering and Environmental Problems*, April 6–10, 2008. Proceedings Environmental and Engineering Geophysical Society, Philadelphia, PA, p. 11.
- Huggenberger, P., Hoehn, E., Beschta, R., Woessner, W., 1996. Abiotic aspects of channels and floodplains in riparian ecology. In: *Workshop on River in the Landscape: Riparian and Groundwater Ecology*. Blackwell Science Ltd., Kastanienbaum, Switzerland, pp. 407–425.
- Hurtig, E., Grosswig, S., Jobmann, M., Kuhn, K., Marschall, P., 1994. Fiber-optic temperature-measurements in shallow boreholes – experimental application for fluid logging. *Geothermics* 23 (4), 355–364.
- Kalbus, E., Reinstorf, F., Schirmer, M., 2006. Measuring methods for groundwater–surface water interactions: a review. *Hydrology and Earth System Sciences* 10 (6), 873–887.
- Kalbus, E., Schmidt, C., Molson, J.W., Reinstorf, F., Schirmer, M., 2009. Influence of aquifer and streambed heterogeneity on the distribution of groundwater discharge. *Hydrology and Earth System Sciences* 13 (1), 69–77.
- Keery, J., Binley, A., Crook, N., Smith, J.W.N., 2007. Temporal and spatial variability of groundwater–surface water fluxes: development and application of an analytical method using temperature time series. *Journal of Hydrology* 336 (1–2), 1–16.
- Kurashima, T., Horiguchi, T., Tateda, M., 1990. Distributed-temperature sensing using stimulated Brillouin-scattering in optical silica fibers. *Optics Letters* 15 (18), 1038–1040.
- Lagarias, J.C., Reeds, J.A., Wright, M.H., Wright, P.E., 1998. Convergence properties of the Nelder–Mead simplex method in low dimensions. *SIAM Journal on Optimization* 9 (1), 112–147.
- Lapham, W.W., 1989. Use of Temperature Profiles Beneath Streams to Determine Rates of Vertical Ground-Water Flow and Vertical Hydraulic Conductivity. US Geological Survey Water Supply Paper 233. US Geological Survey, Denver, CO 35.
- Lowry, C.S., Walker, J.F., Hunt, R.J., Anderson, M.P., 2007. Identifying spatial variability of groundwater discharge in a wetland stream using a distributed temperature sensor. *Water Resources Research* 43 (10), 9.
- Schmidt, C., Conant, B., Bayer-Raich, M., Schirmer, M., 2007. Evaluation and field-scale application of an analytical method to quantify groundwater discharge using mapped streambed temperatures. *Journal of Hydrology* 347 (3–4), 292–307.
- Schön, J.H., 1998. *Physical Properties of Rocks Fundamentals and Principles of Petrophysics*, second ed. Pergamon, Oxford, pp. 583.
- Schwarzenbach, R.P., Westall, J., 1981. Transport of non-polar organic compounds from surface-water to groundwater – laboratory sorption studies. *Environmental Science & Technology* 15 (11), 1360–1367.
- Selker, J.S. et al., 2006a. Distributed fiber-optic temperature sensing for hydrologic systems. *Water Resources Research* 42 (12), 8.
- Selker, J., van de Giesen, N., Westhoff, M., Luxemburg, W., Parlange, M.B., 2006b. Fiber optics opens window on stream dynamics. *Geophysical Research Letters* 33 (24), 4.
- Silliman, S.E., Booth, D.F., 1993. A analysis of time-series measurements of sediment temperature for identification of gaining vs. losing portions of Juday-Creek, Indiana. *Journal of Hydrology* 146 (1–4), 131–148.
- Stallman, R.W., 1965. Steady 1 – dimensional fluid flow in a semi-infinite porous medium with sinusoidal surface temperature. *Journal of Geophysical Research* 70 (12), 2821–2827.
- Storey, R.G., Howard, K.W.F., Williams, D.D., 2003. Factors controlling riffle-scale hyporheic exchange flows and their seasonal changes in a gaining stream: a three-dimensional groundwater flow model. *Water Resources Research* 39 (2), 17.
- Suzuki, S., 1960. Percolation measurements based on heat flow through soil with spherical reference to paddy fields. *Journal of Geophysical Research* 65 (9), 2883–2885.
- Triska, F.J., Duff, J.H., Avanzino, R.J., 1993. The role of water exchange between a stream channel and its hyporheic zone in nitrogen cycling at the terrestrial aquatic interface. *Hydrobiologia* 251 (1–3), 167–184.
- Tyler, S.W. et al., 2009. Environmental temperature sensing using Raman spectra DTS fiber-optic methods. *Water Resources Research*, 45 11.
- vanGenuchten, M.T., 1985. A general approach for modeling solute transport in structured soils. *IAH Memoirs*, 17 513–526.
- Westhoff, M.C. et al., 2007. A distributed stream temperature model using high resolution temperature observations. *Hydrology and Earth System Sciences* 11 (4), 1469–1480.
- Woessner, W.W., 2000. Stream and fluvial plain ground water interactions: rescaling hydrogeologic thought. *Ground Water* 38 (3), 423–429.
- Wroblicky, G.J., Campana, M.E., Valett, H.M., Dahm, C.N., 1998. Seasonal variation in surface–subsurface water exchange and lateral hyporheic area of two stream–aquifer systems. *Water Resources Research* 34 (3), 317–328.
- Young, P.C., Pedregal, D.J., Tych, W., 1999. Dynamic harmonic regression. *Journal of Forecasting* 18 (6), 369–394.
- Young, P.C., Taylor, C.J., Tych, W., Pedregal, D.J., 2007. The Captain Toolbox Centre for Research on Environmental Systems and Statistics. Lancaster University, UK. <www.es.lancs.ac.uk/cres/captain>.